Square vortex solitons with a large angular momentum

Humberto Michinel, José R. Salgueiro, and María J. Paz-Alonso
Área de Óptica, Facultade de Ciencias de Ourense, Universidade de Vigo, As Lagoas s/n, Ourense ES-32005, Spain
(Received 18 December 2003; revised manuscript received 9 July 2004; published 6 December 2004)

We show the existence of square-shaped optical vortices with a large value of the angular momentum hosted in finite-size laser beams which propagate in nonlinear media with a cubic-quintic nonlinearity. The light profiles take the form of rings with sharp boundaries and variable sizes depending on the power carried. Our stability analysis shows that these light distributions remain stable when they propagate, probably for unlimited values of the angular momentum, provided the hosting beam is wide enough. This happens if the peak amplitude approaches a critical value which only depends on the nonlinear refractive index of the material. A variational approach allows us to calculate the main parameters involved. Our results add extra support to the concept of surface tension of light beams that can be considered as a trace of the existence of a liquid of light.

DOI: 10.1103/PhysRevE.70.066605 PACS number(s): 42.65.Tg, 42.65.Jx

I. INTRODUCTION

In wave mechanics, a vortex is a screw phase dislocation, or defect [1], where the amplitude of the field vanishes. The phase around the singularity has an integer number of windings, l, which plays the role of an angular momentum. For fields with nonvanishing boundary conditions, this number is a conserved quantity and governs the interactions between vortices as if they were endowed with electrostatic charges [2]. Thus, l is usually called the "topological charge" of the defect.

Vortices are present in very different branches of physics, such as fluid mechanics, superconductivity, Bose-Einstein condensation, astrophysics or laser dynamics [3], among others [4]. In optics [5], a vortex with charge l takes the form of a black spot surrounded by a light distribution. Around the dark hole, the phase varies from zero to $2\pi l$. These defects appear spontaneously in light propagation through turbulent media and can also be produced by appropriately shining a computer-generated hologram [6]. The trace of vortices in a light field is a characteristic "fork-pattern" interferogram produced by superposition with a tilted planar wave.

The first experimental works on optical wavefront dislocations were carried out in the 1980s, in the context of adaptive systems, where phase singularities were a severe problem for image reconstruction techniques [7]. Since then, they have been studied, among other fields, in optical tweezing [8], particle trapping [9], laser cavities [10], optical interconnectors [11], or even to perform N-bit quantum computers [12].

Concerning light vortices in the nonlinear regime [13], the first theoretical work analyzed their stability in Gaussian-like distributions propagating in optical Kerr materials [14]. It was found for a cubic self-focusing refractive index that a beam of finite size will always filament under the action of a phase dislocation. This also applies to saturable self-focusing nonlinearities [15]. On the other hand, vortex states were predicted and found experimentally for self-defocusing materials both in the Kerr case for continuous background [16] and in the saturable case with finite size beams [17].

It was shown in [18] that stable vortex states with $l=1$ can be obtained as stationary states of the propagation of a laser beam through cubic-quintic optical materials [19–21]. This kind of nonlinearity is characterized by the $\chi^{(3)}>0$ and $\chi^{(5)}<0$ components of the nonlinear optical susceptibility and changes from self-focusing to self-defocusing at a given intensity [22]. It has been recently shown that a gas-liquid phase transition takes place in light beams propagating in this type of materials [23].

In this work, we will show that stable vortex states with a huge value of the angular momentum exist and their peak amplitude and propagation constant tend asymptotically, as the beam flux is increased, to values that do not depend on l. In this way, our results are in contradiction with previous work [24], where it was claimed that stable vortex states in finite-size beams exist only for the values $l=1,2$. For $l=3$, a persistent weak instability was found which was also supposed to exist for higher values of the angular momentum.

In the next section, we will analyze the cubic-quintic nonlinear model, finding numerically the stationary states for a wide range of the angular momentum l (up to 50) and describing their particular properties. Then, we will calculate analytically, by means of the variational method, the critical values of the propagation constant and peak amplitude that characterize the domain of existence of vortices. Finally, we will perform an azimuthal stability analysis to determine the domain zone where stable states can be found.

II. THE MODEL

Let us start by writing the equation for laser beam propagation along z in an optical cubic-quintic material. For paraxial propagation, the equation for the beam envelope Ψ is a nonlinear Schrödinger equation (NLSE), which in normalized units takes the form

$$i\frac{\partial \Psi}{\partial z} + \nabla_{\perp}^2 \Psi + (n_2|\Psi|^2 - n_4|\Psi|^4)\Psi = 0, \qquad (1)$$

where $\nabla_{\perp}^2 = r^{-2}\partial^2/\partial\phi^2 + r^{-1}\partial/\partial r + \partial^2/\partial r^2$ is the transverse Laplacian operator in cylindrical coordinates (r,ϕ,z). The real positive constants n_2 and n_4 are given, respectively, by the $\chi^{(3)}>0$ and $\chi^{(5)}<0$ components of the nonlinear optical sus-

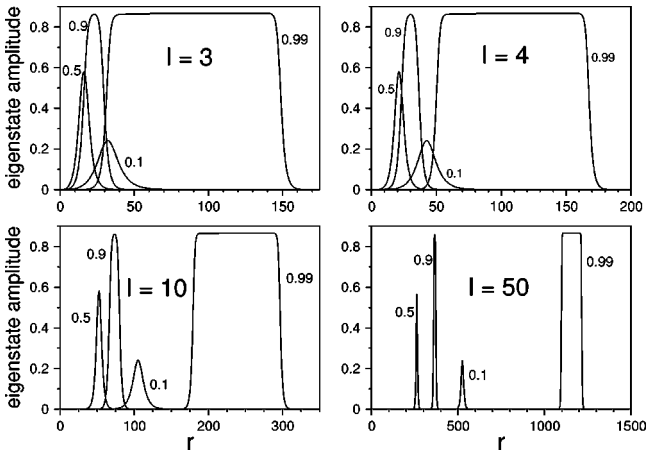

FIG. 1. Numerically calculated radial amplitude profiles of the stationary states of Eq. (3) for $l=3$, 4, 10, and 50 with $\beta/\beta_{cr}=0.1, 0.5, 0.9$, and 0.99. In all the cases $n_2=n_4=1$. Normalized units were used in all the axes.

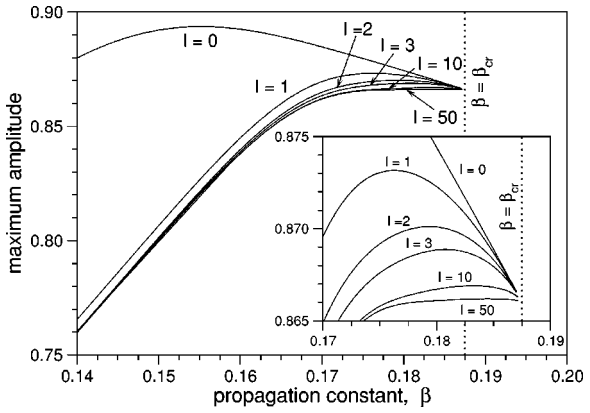

FIG. 2. Maximum amplitude of the stationary states vs propagation constant for angular momenta $l=0, 1, 2, 3, 10$, and 50. All the curves join at the point $A=A_{cr}=0.866$, $\beta=\beta_{cr}=0.1875$. Inset: detail of the zone close to β_{cr} where the calculations become delicate. Normalized units were used in all the axes.

ceptibility and characterize the dependence of the refractive index on the intensity of the beam. If $n_4 \leqslant 0$, a Gaussian beam of high enough power will undergo collapse after self-focusing [25]. The effect of a negative fifth-order susceptibility ($-n_4$ term) combined with diffraction will stop the collapsing tendency for high powers, yielding a stable two-dimensional condensed state of light with surface tension properties similar to those of usual liquids [19,20,23].

We are interested in stationary states with radial symmetry and angular momentum l of the form

$$\Psi(r,\phi,z) = \psi(r)e^{il\phi}e^{i\beta z}, \tag{2}$$

where β is the nonlinear phase shift or propagation constant and $\psi(r)$ is the radial envelope of the field. After substitution of Eq. (2) in Eq. (1), the following z-independent equation is obtained for $\psi(r)$:

$$-\beta\psi + \nabla_r^2\psi - \frac{l^2}{r^2}\psi + n_2\psi^3 - n_4\psi^5 = 0, \tag{3}$$

where $\nabla_r^2 \equiv \partial^2/\partial r^2 + (1/r)\,\partial/\partial r$ is the radial part of the Laplace operator.

For a given integer value of l, a continuum of eigenstates with $\psi \to 0$ as $r \to \infty$ can be obtained by solving numerically Eq. (3). Close to the origin, the shapes follow the linear regime with $\psi \propto r^l$. To this aim, we have used a standard relaxation technique. The profiles of the eigenstates for several values of l and β are plotted in Fig. 1 for the case of $n_2=n_4=1$. We particularly show states with $l=3$ and $l=4$ since these were previously found unstable in previous work [24], as well as two examples of large angular momentum states ($l=10$ and $l=50$). In all cases, the stationary states can only be found for values of β between zero and a fixed critical value β_{cr} [18], which does not depend on l.

It can be appreciated in the graphs that values of β below $0.5\beta_{cr}$ yield light distributions with smooth and wide Gaussian-like shapes. As β is incremented, the beam flux grows and the spatial profiles narrow, yielding a minimum thickness of the ring of the stationary state for values of β around $0.8\beta_{cr}$, keeping approximately the Gaussian shape. For larger values of the propagation constant, the beam flux grows rapidly with β and the peak amplitude of the distribution saturates due to the effect of n_4, reaching asymptotically the value A_{cr}, which is slightly below the maximum amplitude. Thus, high power beams show spatial light distributions with flatted tops in their profiles, similar to those of hyper-Gaussian functions [26,27].

We must stress the intriguing fact that both β_{cr} and A_{cr} do not depend on the value of the topological charge. This is shown in Fig. 2, where the maximum amplitude has been plotted as a function of β. In the inset, the zone $\beta \approx \beta_{cr}$ can be seen in detail. As can be appreciated, whatever the value of l is, all the curves tend to join at the same point. This means that the critical value of the propagation constant and peak amplitude only depend on the nonlinearity and not on the angular momentum. We will revise this result in our analytical study of the next section.

It also worth mentioning that the central hole increases its size with the topological charge for a fixed value of β, as can be seen comparing the profiles in Fig. 1 for $l=3,4$ with $l=10,50$. This is also clearly shown in Fig. 3, where we plot several eigenstates with values of the angular momentum ranging from $l=1$ up to $l=9$, with propagation constant $\beta=0.95\beta_{cr}$. Besides, if β grows, the radius of the hole increases. As the value of β approaches β_{cr}, the thickness of the external ring grows faster than the internal hole, and the final result takes the asymptotic form of a dark spot surrounded by a larger ring of light of almost constant shape which ends abruptly at a given radius. This behavior can be assessed by looking at Fig. 4, where the dimensions of the internal hole and the ring thickness are plotted versus the propagation constant for the particular case of $l=10$. A logarithmic scale was chosen to highlight that the growth in the ring thickness clearly dominates over the hole radius from a certain value of the propagation constant. In the inset, it is also shown, as an example, one of the stationary states with β very close to β_{cr}, showing the huge ring whose width clearly exceeds the hole radius and presents a practically rectangular shape.

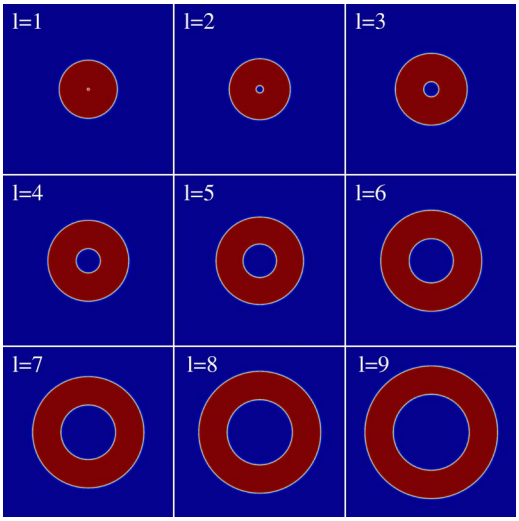

FIG. 3. (Color online) Azimuthal eigenstates of Eq. (2) for $l=1$ to 9 with $\beta=0.95\beta_{cr}$.

III. VARIATIONAL ANALYSIS

To explain the properties of the above light distributions, we have performed a variational analysis [26,27]. It is easy to demonstrate that the stationary system described by the model (3) can be obtained from the following Lagrangian function:

$$\mathcal{L}=r\left\{\left(\frac{d\psi}{dr}\right)^2+\left(\frac{l^2}{r^2}-\beta\right)\psi^2-\frac{n_2}{2}\psi^4-\frac{n_4}{3}\psi^6\right\}. \tag{4}$$

Now assuming a rectangular shape of the stationary states for values of β close to β_{cr} (see Fig. 1), we choose a trial function $\psi_v(r)$ centered at r_0 with amplitude A and width $2w$, given by

$$\psi_v(r)=\begin{cases}A, & |r-r_0|\leqslant w\\ 0, & |r-r_0|>w.\end{cases} \tag{5}$$

Thus r_0, A, and w are the variational parameters. Using this trial function and minimizing the average over the Lagrangian $\langle\mathcal{L}\rangle$ with respect to each parameter [28], we obtain the following conditions:

$$\frac{l^2}{r_0^2-w^2}+\frac{n_2}{2}A^2-\frac{n^4}{3}A^4-\beta=0, \tag{6}$$

$$\frac{l^2}{2r_0w}\ln\left(\frac{r_0+w}{r_0-w}\right)-n_2A^2-n_4A^4+\beta=0, \tag{7}$$

where Eq. (6) is obtained from the minimization with respect to r_0 and w (the same condition is obtained for both parameters), and Eq. (7) follows from minimization with respect to parameter A. In the limit when $\beta\to\beta_{cr}$, the first term of both equations vanishes. This follows by taking into account that $r_0>w$ should always be satisfied (otherwise there would be no hole). Then we have $r_0^2-w^2>r_0^2\to\infty$ and $(r_0^2-w^2)^{-1}\to 0$, consequently the first term of Eq. (6) is zero. For Eq. (7), the argument of the logarithm tends to infinity as it is easily deduced from the fact that the ring width grows faster than the hole radius and $r_0>w$ $[(r_0+w)/(r_0-w)>2w/(r_0-w)\to\infty]$. However, this term diverges logarithmically, meanwhile the denominator goes to infinity quadratically (product r_0w), and consequently the whole term tends to zero. Finally, we can solve the equations for A_{cr} and β_{cr} to obtain

$$A_{cr}=\left(\frac{3n_2}{4n_4}\right)^{1/2}, \tag{8}$$

$$\beta_{cr}=\frac{3n_2^2}{16n_4}. \tag{9}$$

For the particular case considered in the numerical calculations displayed in Figs. 1 and 2, i.e., taken $n_2=n_4=1$, the values obtained for the critical parameters are $A_{cr}=0.866\,025$ and $\beta_{cr}=0.1875$. The comparison of these analytical results with the numerical calculations shows an excellent agreement, since both values are exactly those guessed numerically (see Fig. 2). This good result is due to the choice of the trial function, which fits almost exactly with the numerical solution for values close to the critical point.

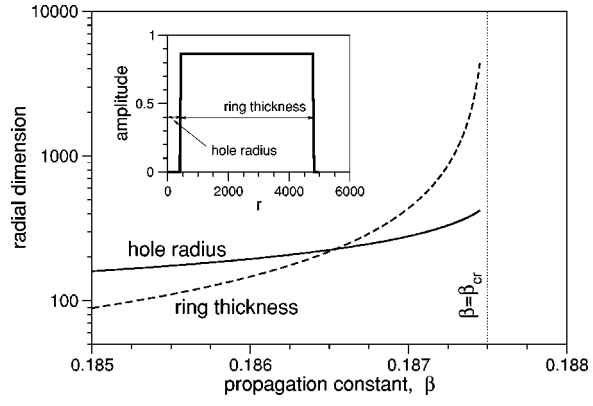

FIG. 4. Dependence of the internal hole radius (continuous line) and ring thickness (dashed line) with the propagation constant β in the vicinity of β_{cr} for eigenstates with $l=10$. Inset: example of a stationary state with $l=10$ and $\beta=0.9998\beta_{cr}$. Normalized units were used in all the axes.

IV. STABILITY ANALYSIS

In order to test the stability of the stationary states, we calculated the growth rates of small azimuthal perturbations to find out the value of β at which they vanish. Additionally, in order to assess the accuracy of the previous analysis, we propagated some *unstable* eigenstates with a split-step Fourier method and found their splitting distances. The inverse of these values should coincide, except for a constant scale factor, with the dominant perturbation eigenvalues calculated in the azimuthal instability analysis. Finally, we have also simulated other kinds of perturbations such as total reflection at the boundary between a cubic-quintic material and air. As we will see below, the eigenstates show robust behavior against these collisions and preserve their angular momentum, although strong oscillations are observed.

To carry out the perturbation analysis, we add to the original eigenstate a small p-order azimuthal perturbation function [15,29],

$$\tilde{\Psi}(r,\phi,z) = [\psi(r) + f(r,z)e^{ip\phi} + h(r,z)e^{-ip\phi}]e^{i(l\phi+\beta z)}, \tag{10}$$

where $f(r,z)$ and $h(r,z)$ are the small complex components of the eigenstate of the p-order azimuthal perturbation. Our interest is to seek those functions which grow exponentially with z, so we assume that they have the form

$$f(r,z) = [f_1(r) + if_2(r)]e^{\delta_p z}, \tag{11}$$

$$h(r,z) = [h_1(r) + ih_2(r)]e^{-\delta_p^* z}, \tag{12}$$

where the parameter δ_p is the perturbation eigenvalue. In this way, the real part of δ_p constitutes the growth rate of this perturbation. If we replace the perturbed eigenstate [Eq. (10)] into Eq. (1) and keep only the first-order terms in $f(r,z)$ and $h(r,z)$ (linearization), we obtain the following set of coupled differential equations for those components $f(r,z)$ and $h(r,z)$:

$$i\frac{\partial f}{\partial z} + \nabla_r^2 f - \frac{(l+p)^2}{r^2}f + Q(\psi)f + R(\psi)h^* = 0, \tag{13}$$

$$i\frac{\partial h}{\partial z} + \nabla_r^2 h - \frac{(l-p)^2}{r^2}h + Q(\psi)h + R(\psi)f^* = 0, \tag{14}$$

where $Q(\psi) \equiv -\beta + (2n_2 - 3n_4|\psi|^2)|\psi|^2$ and $R(\psi) \equiv (n_2 - 2n_4|\psi|^2)|\psi|^2$. The solution of this equation system is obtained using a Crank-Nicholson scheme to propagate an initial arbitrary guess until the shape of each component does not change perceptibly [29]. According to the component dependence on z [Eq. (11)], the value of the growth rate can be calculated at each propagation step by

$$\mathrm{Re}\ \delta_p = \frac{1}{2\Delta z}\ln\frac{|f(r,z+\Delta z)|^2}{|f(r,z)|^2}, \tag{15}$$

where Δz is the propagation step and the function $f(r,z)$ is evaluated in a fixed point r, usually that which corresponds to the maximum. Besides, the functions can be rescaled at each step by this maximum value to avoid an overflow. The propagation is carried out until the value of the perturbation growth rate does not change any more, which indicates that convergence was reached. This allows us to obtain the growth rates $\mathrm{Re}(\delta_p)$ for different order perturbations versus the propagation constant, as depicted in Fig. 5.

The growth rates for vortices with angular momentum $l=3$ and $l=4$ are shown in Figs. 5(a) and 5(b). As can be seen, all of them fall to zero for a value of β below β_{cr}, which implies the existence of a stability window, in contradiction with previous calculations where all the states with $l>2$ were found to be unstable [24]. Our results show that the maximum growth rate corresponds to perturbation eigenvalues with $p \approx 2l$, which allows us to estimate the number of filaments N resulting from the breakup of the unstable vortices ($N \approx 2l$). Besides this, the perturbation $p=2$ has been proven to be the most persistent, despite the value of the angular momentum. Hence, in Fig. 5(c) we plot the curves associated to this perturbation for different values of the angular momentum, including the cases corresponding to $l=10$ and $l=50$. As can be appreciated in these plots, there exists a window between the vanishing point and the limit value for β ($\beta=\beta_{cr}$), which proves the existence of a stability zone close to the critical point containing an infinite number of stable eigenstates. Note that this window narrows for high values of l but remains finite. As l increases, the point at which the perturbation vanishes approaches asymptotically the critical point. However, we believe that the critical point

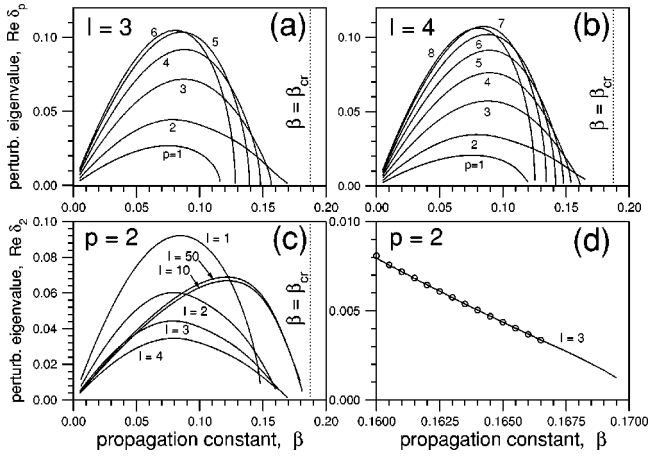

FIG. 5. Growth rate of the azimuthal perturbation vs β. In (a) and (b), the angular momentum is fixed [$l=3$ for (a), $l=4$ for (b)] and the values of the perturbation order p are indicated by labels near the curves. In (c) the growth rate for the perturbations with $p=2$ for $l=1,2,3,4,10$, and 50 are plotted. In (d), a comparison between the inverse of the splitting distance (dots) and $p=2$ perturbation eigenvalue for unstable states with $l=3$ is shown. Normalized units were used in all the axes.

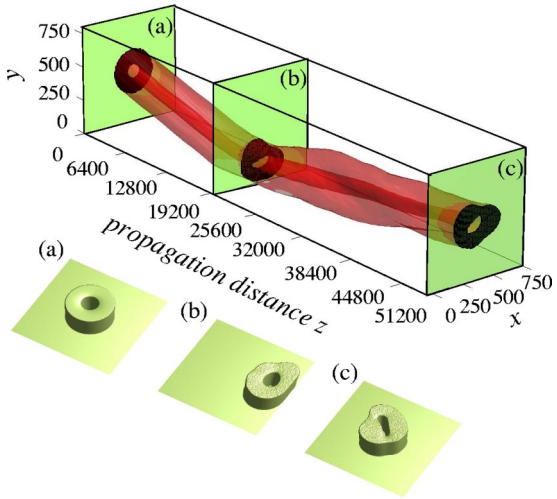

FIG. 6. (Color online) Numerical simulation of the total reflection at a planar boundary between a cubic-quintic and a linear media (air). For this stationary state, the angular momentum is $l=4$ and the propagation constant $\beta=0.95\beta_{cr}$. The top image is an isosurface of the propagating beam. The boundary between the nonlinear material and air is the plane $y=0$. The images (a)–(c) correspond to different transversal cutoffs (intensity profiles) of the beam at different values of the propagation distance z. Normalized units were used in all the axes.

itself is never reached, even for arbitrarily high values of the topological charge.

When β is close to β_{cr}, the azimuthal analysis becomes very delicate and it has to be carried out in a very careful way. In fact, convergence takes a much longer distance, and an erroneous final result is obtained if the number of samples and the propagation step are not chosen appropriately. In this sense, combining the analysis with direct calculations of the splitting distance of the unstable eigenstates is definitively useful. In Fig. 5(d), there is an enlargement of the region of Fig. 5(c) where the perturbation for $l=3$ drops to zero. The points obtained propagating the eigenstates and taking the inverse of the distance where they split are also plotted. These values were subsequently scaled by the same constant value to compare with the perturbation eigenvalue curve. As can be appreciated, the values obtained from these propagation experiments fall to zero with the same slope as the perturbation eigenvalues do. When the stability analysis is not performed with enough accuracy, a more steady behavior of the curve appears, which implies that the eigenvalue falls to zero at a higher value of β. This allows us to assess the validity of the perturbation analysis.

As a final test of the stability of the eigenstates, we have simulated the total reflection at a planar boundary between a cubic-quintic material and air for beams with different angular momenta. For the simulation, we have used a split-step Fourier method with a 520×520 grid. The idea is similar to the test of surface tension properties of "liquid light beams" from Ref. [23]. As can be seen in Fig. 6, a beam with $l=4$ does not split after the total reflection, although a strong oscillation is observed. This is more proof of the stability of these nonlinear waves. We must notice that depending on the incidence angle, a strong deformation of the beam can be induced, which can yield a split or a decay of the inner vortex into several defects with lower topological charges [30].

V. CONCLUSIONS

The main conclusions that can be derived from the present work are the following. First, stable azimuthal finite-size beams with arbitrary very large angular momentum can exist in optical materials with self-focusing (cubic) and defocusing (quintic) nonlinearity. Second, the shapes of these beams tend asymptotically to squarelike ring profiles with bigger dark holes for higher values of the angular momentum. And finally, the critical values of the propagation constant and amplitude do not depend on the angular momentum of the beam.

[1] J. F. Nye and M. V. Berry, Proc. R. Soc. London, Ser. A **336**, 165 (1974).
[2] D. Rozas, Z. S. Sacks, and G. A. Swartzlander, Jr., Phys. Rev. Lett. **79**, 3399 (1997).
[3] N. N. Rosanov, *Spatial Hysteresis and Optical Patterns* (Springer, Berlin, 2002).
[4] L. Pismen, *Vortices in Nonlinear Fields* (Oxford University Press, London, 1999).
[5] Yu. S. Kivshar and G. P. Agrawal, *Optical Solitons: From Fibers to Photonic Crystals* (Academic, San Diego, 2002).
[6] N. R. Heckenberg, R. McDuff, C. P. Smith, and A. G. White, Opt. Lett. **17**, 221 (1992).
[7] N. B. Baranova, B. Ya. Zel'dovich, A. V. Mamaev, N. F. Pilipetslii, and V. V. Shkukov, Pis'ma Zh. Eksp. Teor. Fiz. **33**, 206 (1981) [JETP Lett. **33**, 195 (1981)].
[8] N. B. Simpson, K. Dholakia, L. Allen, and M. J. Padgett, Opt. Lett. **22**, 52 (1997).
[9] K. T. Gahagan and G. A. Swartzlander, Jr., Opt. Lett. **21**, 827 (1996).
[10] C. O. Weiss, M. Vaupel, K. Staliunas, G. Slekys, and V. B. Taranenko, Appl. Phys. B: Lasers Opt. **68**, 151 (1999).
[11] J. Scheuer and M. Orenstein, Science **285**, 230 (1999).
[12] A. Mair, A. Vaziri, G. Weihs, and A. Zeilinger, Nature (London) **412**, 313 (2001).
[13] Yu. S. Kivshar and E. Ostrovskaya, Opt. Photonics News **12**, 24 (2001).
[14] V. I. Kruglov and R. A. Vlasov, Phys. Lett. **111A**, 401 (1985).
[15] W. J. Firth and D. V. Skryabin, Phys. Rev. Lett. **79**, 2450 (1997).
[16] G. A. Swartzlander, Jr. and C. T. Law, Phys. Rev. Lett. **69**, 2503 (1992).
[17] V. Tikhonenko and N. Akhmediev, Opt. Commun. **126**, 108 (1996).
[18] M. Quiroga-Teixeiro and H. Michinel, J. Opt. Soc. Am. B **14**, 2004 (1997).
[19] A. H. Piekara, J. S. Moore, and M. S. Feld, Phys. Rev. A **9**, 1403 (1974).
[20] C. Josserand and S. Rica, Phys. Rev. Lett. **78**, 1215 (1997).
[21] T. A. Davydova and A. I. Yakimenko, J. Opt. A, Pure Appl. Opt. **6**, S197 (2004).
[22] G. Fang, Y. Mo, Y. Song, Y. Wang, C. Li, and L. Song, Opt. Commun. **205**, 337 (2002).
[23] H. Michinel, J. Campo-Táboas, R. García-Fernández, J. R. Salgueiro, and M. L. Quiroga-Teixeiro, Phys. Rev. E **65**, 066604 (2002).
[24] I. Towers, A. V. Buryak, R. A. Samut, B. A. Malomed, L. C. Crasovan, and D. Mihalache, Phys. Lett. A **288**, 292 (2001).
[25] R. Y. Chiao, E. Garmire, and C. H. Townes, Phys. Rev. Lett. **13**, 479 (1964).
[26] K. Dimitrievski, E. Reimhult, E. Svensson, A. Öhgren, D. Anderson, A. Berntson, M. Lisak, and M. L. Quiroga-Teixeiro, Phys. Lett. A **248**, 369 (1998).
[27] M. Quiroga-Teixeiro, A. Berntson, and H. Michinel, J. Opt. Soc. Am. B **16**, 1697 (1999).
[28] D. Anderson, Phys. Rev. A **27**, 3135 (1983).
[29] J. M. Soto-Crespo, D. R. Heatley, E. M. Wright, and N. N. Akhmediev, Phys. Rev. A **44**, 636 (1991).
[30] M. J. Paz-Alonso, D. Olivieri, H. Michinel, and J. R. Salgueiro, Phys. Rev. E **69**, 056601 (2004).